Liquid–Liquid Interfacial Reactors

Deutsche Ausgabe: DOI: 10.1002/ange.201602565
Internationale Ausgabe: DOI: 10.1002/anie.201602565

Isolating Reactions at the Picoliter Scale: Parallel Control of Reaction Kinetics at the Liquid–Liquid Interface

*Gia Chuong Phan-Quang, Hiang Kwee Lee, and Xing Yi Ling**

Abstract: *Miniaturized liquid–liquid interfacial reactors offer enhanced surface area and rapid confinement of compounds of opposite solubility, yet they are unable to provide in situ reaction monitoring at a molecular level at the interface. A picoreactor operative at the liquid–liquid interface is described, comprising plasmonic colloidosomes containing Ag octahedra strategically assembled at the water-in-decane emulsion interface. The plasmonic colloidosomes isolate ultrasmall amounts of solutions (< 200 pL), allowing parallel monitoring of multiple reactions simultaneously. Using the surface-enhanced Raman spectroscopy (SERS) technique, in situ monitoring of the interfacial protonation of dimethyl yellow (p-dimethylaminoazobenzene (DY)) is performed, revealing an apparent rate constant of 0.09 min^{-1} for the first-order reaction. The presence of isomeric products with similar physical properties is resolved, which would otherwise be indiscernible by other analytical methods.*

Colloidosomes are robust spherical microcapsules formed by the self-assembly of nanoparticles on the immiscible liquid–liquid interface during emulsification.[1] They inherit the characteristics of an emulsion system, including a dual-phase nature, large surface area, and remarkable interfacial stability.[2] Additional functionality can be imparted by the choice of nanoparticles used.[3] Notably, an attractive application of colloidosomes is their use as liquid–liquid interfacial picoreactors.[4] At their permeable shells they possess a unique capacity for confinement of multiple reagents of opposite solubility within close proximity.[4b,5] Furthermore, the enhanced interfacial area of such picoreactors facilitates diffusion-limited phase transfer of molecules across an interface,[4b] and improves interfacial reaction efficiency by orders of magnitude compared to macroscopic systems.[2,6] However, a major drawback of current colloidosome reactors is their reliance on ex situ monitoring techniques that cannot offer vital molecular information.[7] Consequently, it is not possible to study the intrinsic reaction dynamics and differentiation of physically similar isomeric species in the native biphasic environment common to colloidosome reactors.

The aforementioned limitations may be tackled with plasmonic colloidosomes, which are excellent three-dimensional (3D) structures constructed from noble metal nanoparticles that are suited to surface-enhanced Raman spectroscopy (SERS).[8] Featuring a high density of intense SERS hot spots, ultrasensitive plasmonic colloidosomes provide specific molecular vibrational fingerprints simultaneously across the immiscible liquids.[8] Their ability to compartmentalize various liquids suggests that they have potential as picoscale reactors for parallel reaction screening.[7,9] Most importantly, they enable in situ tracking of molecular events directly at the native liquid–liquid interface, which is crucial for elucidating reaction kinetics and mechanisms,[10] and ultimately allows the discovery and optimization of new reaction pathways in synthetic chemistry.[11]

Herein, we describe fabrication of Ag octahedra-stabilized plasmonic colloidosomes for use in confinement of picoliter volumes of liquids, allowing control of parallel reaction kinetics in multiple liquid–liquid interfacial reactions. Our model reaction is the interfacial protonation of DY across the decane–water interface. Together with computational density functional theory (DFT) simulations, our in situ SERS highlights the unprecedented successful differentiation and quantification of two isomeric products, exemplifying the superiority of plasmonic colloidosomes compared to conventional high performance liquid chromatography (HPLC) techniques for resolving physically similar isomers. Correspondingly, the reaction order and its kinetics are determined by evaluating the consumption of H^+ protons over a number of trials at various pH values, which showcases the quantitative nature of SERS measurements carried out on plasmonic colloidosomes. We also demonstrate the high throughput monitoring of interfacial reactions on multiple colloidosomes placed in a single organic phase.

Ag octahedra nanoparticles of 350 ± 40 nm (Supporting Information, Figure S1) are used as encapsulating solids for the fabrication of plasmonic colloidosomes because of their highly efficient light scattering effect.[12] Colloidosomes are prepared by intense emulsification of an aqueous droplet (microliter) in a colloidal decane suspension of hydrophobic perfluorodecanethiol-grafted Ag octahedra (Figure 1 A). The as-formed spherical colloidosomes exhibit an average diameter of 72 ± 20 μm (Figure 1 B) with closely packed plasmonic shells comprising five (± 1) layers of Ag octahedra (Figure 1 C,D). Furthermore, plasmonic colloidosomes demonstrate the strongest SERS behavior at their Ag shell, which is capable of sensing methylene blue down to an approximately 20 attomole level (Figure 1 E–G), corresponding to

[*] G. C. Phan-Quang, H. K. Lee, Prof. X. Y. Ling
Division of Chemistry and Biological Chemistry, School of Physical and Mathematical Sciences, Nanyang Technological University
50 Nanyang Avenue, Singapore 637371 (Singapore)
E-mail: xyling@ntu.edu.sg
H. K. Lee
Institute of Materials Research and Engineering, Agency for Science, Technology and Research (A*STAR)
2 Fusionopolis Way, Innovis, #08-03, Singapore 138634 (Singapore)
Supporting information and the ORCID identification number(s) for the author(s) of this article can be found under http://dx.doi.org/10.1002/anie.201602565.

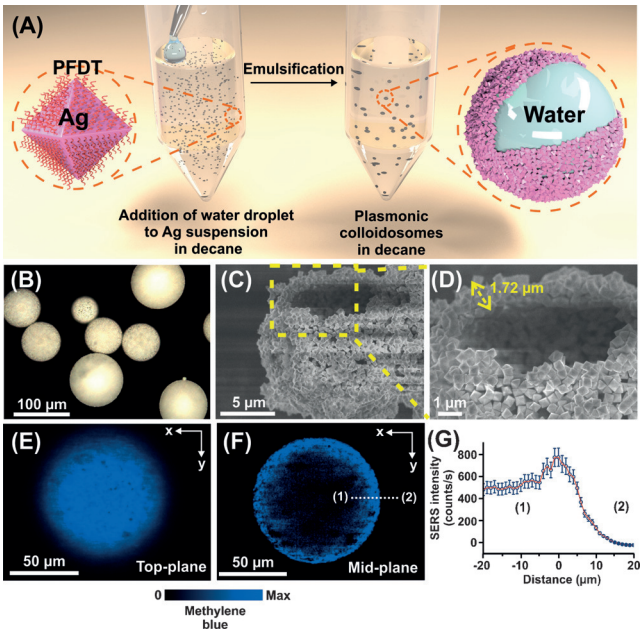

Figure 1. Fabrication and characterization of plasmonic colloidosomes. A) Formation of plasmonic colloidosomes with PFDT-grafted (PFDT = perfluorodecanethiol) Ag octahedra and their B) microscopic images. SEM images of C) a hollow colloidosome shell and D) the magnified segment of the dashed yellow box in (C). x–y SERS images of a colloidosome encapsulating methylene blue (10^{-6} M) when a laser is focused on the E) top and F) mid-plane of the particle. G) SERS intensity–distance profile along the white dotted line of (F), from (1) to (2).

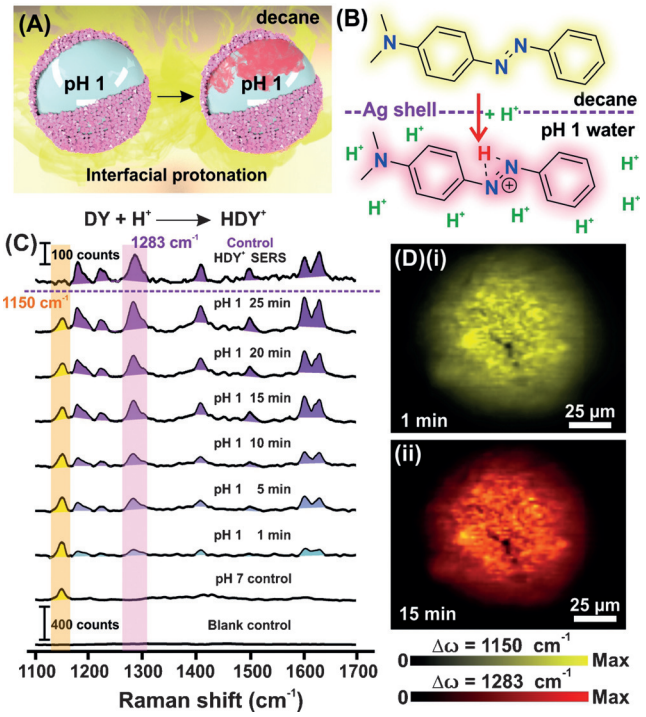

Figure 2. Interfacial protonation of DY across the colloidosome shell. A) Interfacial protonation of DY (DY—yellow) to form protonated DY (HDY^+—red) on colloidosomes encapsulating a pH 1 solution. B) Molecular depiction of interfacial protonation of DY across the liquid–liquid interface. C) SERS spectra recorded over time for colloidosomes encapsulating a pH 1 solution submerged in a DY (10^{-2} M) solution in decane. Blank control refers to a colloidosome encapsulating a solution of the same pH in pure decane. HDY^+ SERS spectra are obtained with a colloidal Ag solution. $\nu(C{-}N_{azo})_{DY} = 1150\ cm^{-1}$ (orange band), $\nu(N{=}N)_{HDY} = 1283\ cm^{-1}$ (purple band). D) SERS images of a colloidosome encapsulating a pH 1 solution in a DY solution at (i) 1 min and (ii) 15 min; both the DY 1150 cm^{-1} (yellow-indexed) and HDY 1283 cm^{-1} (red-indexed) signals are specified.

an analytical enhancement factor of 10^5 (Supporting Information, Figure S2). This characteristic is attributed to the high density of intense SERS hot spots arising from closely packed Ag octahedra clusters across the 3D surface of the colloidosome. As a consequence of the size-independent SERS sensitivity of plasmonic colloidosomes, we use structures with a diameter of 72 ± 20 μm (corresponding to ca. 195 pL) to perform our subsequent interfacial reaction experiments.[8]

Plasmonic colloidosomes are used to conduct a miniaturized interfacial protonation of DY at the decane–water interface (Figure 2). We aim to demonstrate that plasmonic colloidosomes possess dual-functionality as 1) a permeable picoreactor for liquid–liquid interfacial reaction, as well as 2) an in situ SERS monitoring platform. The reaction involves the protonation of DY (yellow; dissolved in the organic solvent decane), forming protonated DY (red HDY^+; soluble in water) at the liquid–liquid interface, followed by the diffusion of HDY^+ into the encapsulated aqueous phase (Supporting Information, Figure S3A). Notably, the interfacial protonation of DY only happens at pH values lower than the pK_a of DY at 3.3.[13] Such interfacial protonation reactions are important and are widely applied as a separation technique to extract organic molecules from the organic phase into the aqueous phase, allowing purification or characterization of organic materials.[14] However, there has been no report on the quantitative examination of the kinetics and molecular events occurring at the native interfacial reaction site.

Aiming to investigate reaction kinetics and molecular information, we conduct our in situ SERS experiments with time-dependent x–y SERS imaging using a laser focused on the top of the colloidosome over 25 min (Figure 2C; Supporting Information, Figure S4). Briefly, colloidosomes encapsulating aqueous pH 1 or pH 7 solutions are immersed in a decane solution containing excess DY (10^{-2} M). A control experiment using colloidosome in pH 7 exhibits a consistent band at 1150 cm^{-1} over the entire reaction duration,[15] which is the fingerprint C-N stretching mode of DY and indicates no observable formation of HDY^+ (Figure 2C). Upon adjustment to the pH 1 colloidosome, the SERS spectrum clearly evolves new vibrational features at 1283 and 1633 cm^{-1}, which are attributed to the N=N and C=C stretching modes of HDY^+.[15] The SERS image of a pH 1 colloidosome prior to the reaction only shows a 1150 cm^{-1} signal corresponding to DY (yellow-indexed), whereas the SERS profile of the same colloidosome after 15 min of reaction is overwhelmed by the HDY^+ signature peak (red-indexed) at 1283 cm^{-1} (Figure 2D). This behavior is attributed to the protonation of DY by H^+ at the liquid–liquid interface, generating protonated HDY^+ ions that gradually penetrate from the interface

into the encapsulated aqueous phase (pH 1; Supporting Information, Figure S3). This observation agrees with our control set-up, involving bulk biphasic protonation of DY. Hence, we affirm the shell permeability of plasmonic colloidosomes and exemplify their capacity for compartmentalization of reactants, thereby enabling interfacial reactions involving dynamic diffusion of molecules across the liquid–liquid interface.

Plasmonic colloidosomes also excel at the in situ resolution of isomer structures. Asymmetry is observed in all the HDY^+ SERS features in pH 1 colloidosomes (Figure 3A,B). Generally, each asymmetric peak can be attributed to the presence of two contributing peaks (Figure 3A). In particular, the C–H wagging mode at 1180 cm^{-1} comprises 1178 and 1190 cm^{-1} peaks, the C–N stretching mode at 1220 cm^{-1} includes 1220 and 1229 cm^{-1} bands, and the N=N stretching mode at 1283 cm^{-1} is comprised of 1281 and 1305 cm^{-1} signals (Figure 3A). These results reveal the presence of two isomeric products in the DY protonation reaction, which possess similar vibrational profiles that overlap with each other. In combination with our DFT simulations, we attribute this observation to the two potential protonation sites in the DY molecule, each of which is situated at one of the N=N azo nitrogen atoms (labeled HDY^+(N1) and HDY^+(N2); red circles in Figure 3C) because of their large coefficients in the two highest occupied molecular orbitals (HOMO; Supporting Information, Figure S5A). They are also the most electron-rich atoms (Supporting Information, Figure S5B), and possess the strongest affinity for H^+ protons according to Pearson's hard and soft acids and bases theory.[16]

Additionally, DFT simulations affirm the protonation of the azo nitrogen atoms of DY to form isomeric HDY^+(N1) and HDY^+(N2) (Figure 3C). The simulated SERS spectra of both HDY^+ isomers demonstrate the same characteristic vibrational modes as that presented by HDY^+, with slight differences in vibrational energies: C–H wagging modes at 1204 and 1197 cm^{-1}, C–N stretching modes at 1249 and 1232 cm^{-1}, N=N stretching modes at 1320 and 1324 cm^{-1}, for HDY^+(N1) and HDY^+(N2), respectively (Figure 3B; Supporting Information, Table S3). This agreement with the experimental spectra clearly indicates the presence of both protonation isomeric products HDY^+(N1) and HDY^+(N2), which have not yet been resolved in reported SERS studies of this molecule.[15] Importantly, the normal Raman spectrum of HDY^+ (in the absence of any Ag particles) exhibits identical peak asymmetry (Supporting Information, Figure S7), which confirms that asymmetry does indeed arise from the presence of two isomers of HDY^+, rather than from different absorption configurations of HDY^+ on the Ag surface. An isomeric ratio analysis is performed on the basis of the C–N stretching mode of HDY^+ at 1220 cm^{-1}, which comprises two signals at 1220 and 1229 cm^{-1} assigned to HDY^+(N2) and HDY^+(N1) isomers, respectively (Supporting Information, Figure S6 and Table S3). This feature is also located in a clear window free from DY SERS interference. Notably, we observe a constant 1.5 ± 0.2 relative contribution ratio of HDY^+(N2)/HDY^+(N1) throughout the reaction duration (Figure 3D). This relative contribution ratio is generally constant for other characteristic vibrational modes of HDY^+ (Supporting Information, Figure S8). In fact, the relative SERS contribution ratio is an excellent measure by which the progress of the reaction may be monitored.[17] The constant SERS contribution ratio indicates that the isomeric products of HDY^+ are directly formed in a thermodynamically determined ratio from the start of the reaction.[18] This characteristic can be vital in asymmetric synthesis, where mixtures of isomeric products are common but remain indiscernible by chromatography techniques.[19] We also highlight the superiority of plasmonic colloidosomes compared to the HPLC technique: the latter is unable to resolve the aforementioned isomers, which possess highly similar structures and physical properties (Supporting Information, Figure S9).

Elucidation of critical reaction dynamics with the aid of plasmonic colloidosomes is further demonstrated by quantitative investigation of the

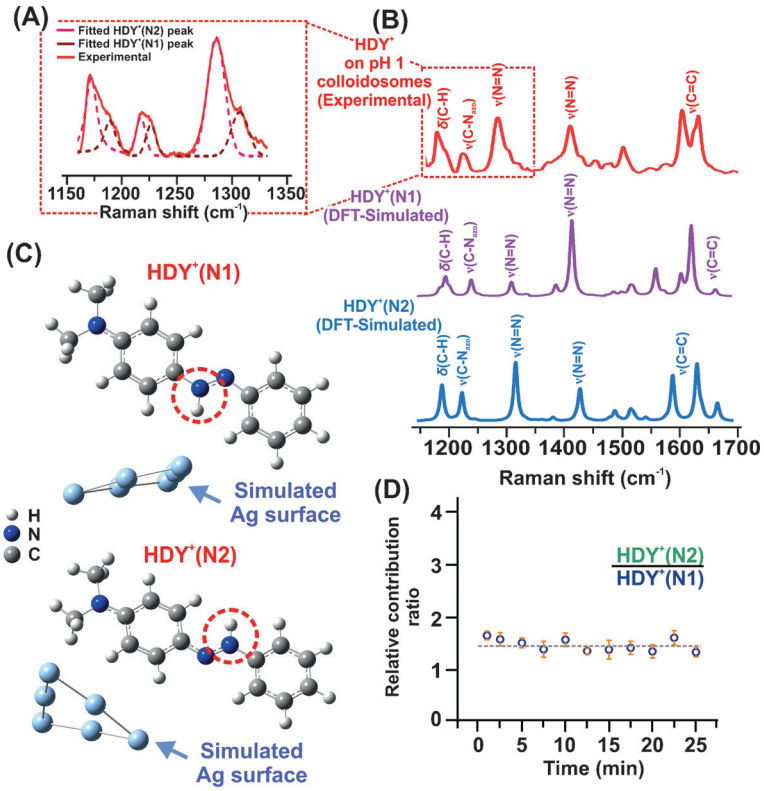

Figure 3. Interpretation of SERS spectra of DY and HDY^+, including likely molecular structures and interactions with Ag. A) Magnified spectrum of the dotted region in the "HDY^+ on pH 1 colloidosomes" spectrum in (B). Peaks pertaining to the two protonated isomers of HDY^+ are fitted. B) SERS spectra of HDY^+ observed on colloidosomes encapsulating a pH 1 solution submerged in a DY solution for 15 min. DFT-simulated SERS spectra of both isomers of HDY^+ are depicted for comparison. C) Molecular structures of both isomers of HDY^+ with an Ag-6 cluster (for SERS simulation) optimized by DFT-simulation. D) Relative ratio of contributions from the fitted C–N stretching mode at 1220 cm^{-1} (experimental peak in the HDY^+ spectra) with respect to time.

temporal evolution of the HDY^+ product in situ at the liquid–liquid interface. We would like to emphasize that SERS intensity measured at the colloidosome shell is accurate for the kinetic modelling of the chemical species in both phases because of their fast diffusion rate over the ultrasmall droplet volume (Supporting Information). Briefly, interfacial protonation of DY is described by Equation (1),

$$DY_{(org)} + H^+_{(aq)} \xrightarrow{k} HDY^+_{(aq)} \quad (1)$$

where k is the rate constant of our model interfacial reaction.

We treat [DY] as a constant, since there is a 10^6-fold excess of DY (2.5×10^{-5} mol) in the external organic phase compared to H^+ in the encapsulated aqueous phase (2.0×10^{-11} mol), as indicated by the constant intensity of the DY 1150 cm^{-1} C–N stretching SERS band at 1510 ± 160 counts (Supporting Information, Figure S10). Notably, the H^+ proton is Raman inactive, hence we use the SERS responses of HDY^+ to achieve time-dependent profiling of H^+ consumption. The formation of HDY^+ product is tracked on the basis of the relative intensity (R_t) of the HDY^+ SERS signal (at 1283 cm^{-1}) against the constant SERS intensity of DY (at 1150 cm^{-1}) at time (t) [Eq. (2)]. This strategy minimizes errors arising from experimental fluctuations.

$$R_t = \frac{I_{1283\,cm^{-1},t}}{I_{1150\,cm^{-1},t}} = \frac{\alpha_{HDY}[HDY^+]_t}{\alpha_{DY}[DY]} = c[HDY^+]_t, \quad \text{where } c = \frac{\alpha_{HDY}}{\alpha_{DY}[DY]} \quad (2)$$

and α_{HDY} and α_{DY} (counts L mol^{-1}) are specific activity constants of HDY^+ and DY, respectively (Supporting Information). To ascertain the $[H^+]$ necessary for the determination of k_{app}, we assume that all $[H^+]$ is consumed on conversion of DY into HDY^+. Subsequently, we used the infinity quantity method to relate the product formation profile to the reactant consumption (based on the difference of a physical quantity of the product at time infinity (∞) and a specific time (t); see Supporting information) to indirectly extract the consumption profile of H^+ with respect to the production of HDY^+ [Eq. (3)].[18]

$$c[H^+]_t = R_\infty - R_t = 4.6 - R_t \quad (3)$$

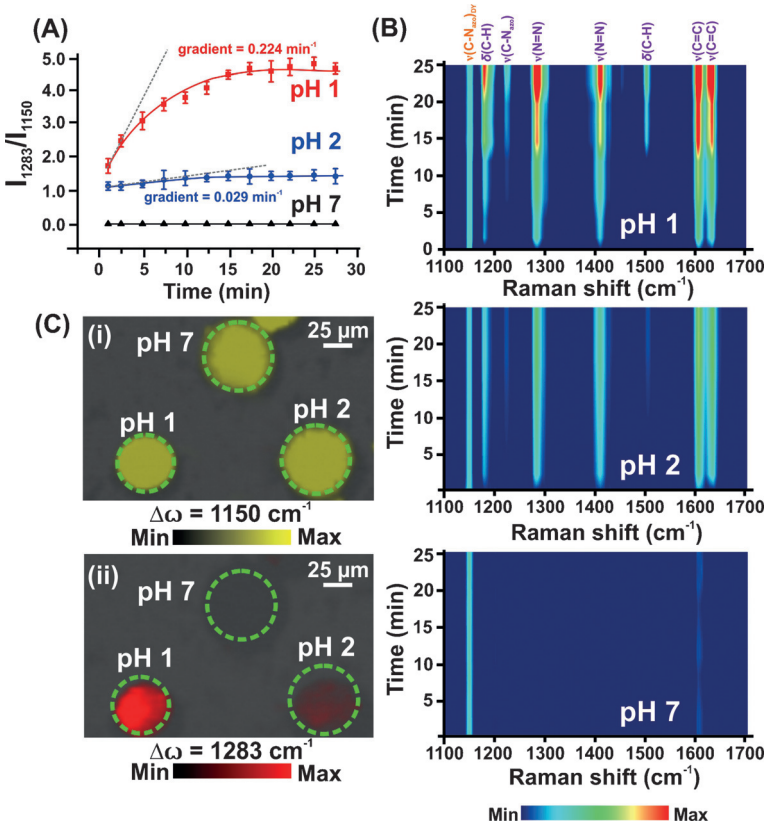

Figure 4. The formation of HDY^+ at different pH values. A) Area ratio of peak intensities, I_{1283}/I_{1150}. B) Time-resolved maps of the SERS spectra on the colloidosomes pH 1, pH 2, and pH 7 submerged in a DY (10^{-2} M) solution over time. C) SERS images of a mixture of pH 1, pH 2, and pH 7 colloidosomes submerged in a DY solution for 15 min. (i) 1150 cm^{-1} (yellow-indexed); (ii) 1283 cm^{-1} (red-indexed); in the case of the 1283 cm^{-1} shift, pH 1 colloidosomes exhibit strong signals, pH 2 colloidosomes show weak signals, and pH 7 colloidosomes show no response.

where c denotes the proportionality constant in this relationship, which correlates with the aforementioned variable c in Equation (2). R_∞ and R_t are the relative SERS intensities of HDY^+/DY at infinity and time (t), respectively (Figure 4 A). R_∞ remained constant at 4.6 ± 0.5 beyond 15 min of reaction (Figure 4 A, B). Our derivation leads to the following relationship between ($4.6-R_t$) in Equation (4),

$$ln\, c\,[H^+] = ln\,(4.6-R_t) = -k_{app}t + A, \quad (4)$$

where the reaction obeys first-order rate law (reaction order is discussed in the Supporting Information), and $A = ln\,[H^+]_0 + ln\,c$.

Using Equation (4), a linear relationship is indeed evident in a plot of $\ln(4.6-R_t)$ against reaction time (t), which verifies that the formation of HDY^+ obeys first-order kinetics with respect to H^+ (Supporting Information, Figure S12). Determination of the gradient of a plot of $\ln(4.6-R_t)$ against reaction time (t), reveals that the apparent rate constant (k_{app}) of our model interfacial reaction is 0.09 min^{-1}, which agrees with the value obtained at pH 2 (Supporting Information, Figure S13). Similar reaction kinetic are determined using other HDY^+ vibrational modes, such as the C=C stretching mode at 1633 cm^{-1} (Supporting Information, Figure S14). Notably, we observe consistent kinetic profiles by measuring the SERS spectra at the half-plane of the colloidosome (Supporting Information, Figure S15), which illustrates the advantage of plasmonic colloidosomes as a 3D SERS platform.

Plasmonic colloidosomes enable high throughput SERS monitoring of multiple interfacial reactions on colloidosomes. Colloidosomes encapsulating pH 1, pH 2, and pH 7 solutions are monitored simultaneously but independently as isolated picoreactors in the same DY solution (Figure 4A,C). All colloidosomes respond to DY similarly in the external phase (labeled yellow) and exhibit a uniform 1150 cm^{-1} SERS intensity for DY throughout the reaction (Figure 4B,C). Notably, pH 1 colloidosomes exhibit the steepest growth profile for HDY^+ signals (Figure 4B), which is also illustrated in our color-indexed SERS image where the pH 1 colloidosome is brightly lit when the HDY^+ 1283 cm^{-1} signal is selected (labeled red, Figure 4C(ii)). By comparison, pH 2 colloidosomes display an approximately five-fold weaker red color intensity, as observed in the same SERS image. We observe an approximately 10-fold slower initial formation rate of HDY^+ in pH 2 colloidosomes relative to that for pH 1 colloidosomes (initial gradients of R_I vs. time plot: 0.224 min^{-1} and 0.029 min^{-1} for pH 1 and pH 2, respectively),[18] which obeys the first-order kinetics of our model interfacial reaction (rate $= k_{app}[H^+]$; Figure 4A; Supporting Information, Figure S16). On the contrary, control pH 7 colloidosomes do not exhibit observable HDY^+ signals in the SERS spectrum and remained invisible in the SERS image of HDY^+ (Figure 4C(ii)). We exclude errors resulting from cross-talking between closely spaced plasmonic colloidosomes,[8] as well as those arising from SERS activity arising from pH-induced effects on the Ag shell (Supporting Information, Figure S17). Our results therefore emphasize the importance of colloidosome robustness for achieving efficient isolation of reactions intended for high throughput reaction monitoring.

In conclusion, we have fabricated plasmonic colloidosomes from Ag octahedra that are responsive to SERS. These particles are dual-phase picoreactors for simultaneous in situ reaction monitoring and molecular analysis of liquid–liquid interfacial reactions, which are applied in the decane–water interfacial protonation of DY on an ultrasmall droplet (< 200 pL). Our technique excels at distinguishing 1) the protonated isomers of HDY^+ in a constant thermodynamic ratio, and 2) the pseudo first-order kinetics of the reaction with an apparent rate constant of 0.09 min^{-1} (as retrieved from in situ SERS monitoring of the reaction progress). Parallel reaction monitoring is performed with plasmonic colloidosomes, demonstrating their potential benefits as picoreactors for high throughput screening of reactions involving multiple components that are soluble in a single- or dual-phase solvent. Coupled with a SERS measurement technique, plasmonic colloidosomes offer multiple advantages for small-scale study of interfacial phenomena commonly encountered in the fields of food chemistry, clinical analysis, and drug treatment.

Acknowledgements

X.Y.L. thanks Singapore National Research Foundation (NRF-NRFF2012-04) for support. G.C.P.-Q acknowledges support from a Nanyang Presidential Graduate Scholarship. H.K.L thanks the A*STAR graduate scholarship from A*STAR, Singapore.

Keywords: colloidosomes · high throughput · in situ surface-enhanced Raman spectroscopy (SERS) · isomer identification · picoreactors

How to cite: *Angew. Chem. Int. Ed.* **2016**, *55*, 8304–8308
Angew. Chem. **2016**, *128*, 8444–8448

[1] A. D. Dinsmore, M. F. Hsu, M. G. Nikolaides, M. Marquez, A. R. Bausch, D. A. Weitz, *Science* **2002**, *298*, 1006–1009.
[2] Z. Wang, M. C. M. van Oers, F. P. J. T. Rutjes, J. C. M. van Hest, *Angew. Chem. Int. Ed.* **2012**, *51*, 10746–10750; *Angew. Chem.* **2012**, *124*, 10904–10908.
[3] M. Li, R. L. Harbron, J. V. M. Weaver, B. P. Binks, S. Mann, *Nat. Chem.* **2013**, *5*, 529–536.
[4] a) S. Crossley, J. Faria, M. Shen, D. E. Resasco, *Science* **2010**, *327*, 68–72; b) K. Piradashvili, E. M. Alexandrino, F. R. Wurm, K. Landfester, *Chem. Rev.* **2016**, *116*, 2141–2169.
[5] R. Ameloot, F. Vermoortele, W. Vanhove, M. B. J. Roeffaers, B. F. Sels, D. E. De Vos, *Nat. Chem.* **2011**, *3*, 382–387.
[6] a) C. Huo, M. Li, X. Huang, H. Yang, S. Mann, *Langmuir* **2014**, *30*, 15047–15052; b) C. Vázquez-Vázquez, B. Vaz, V. Giannini, M. Pérez-Lorenzo, R. A. Alvarez-Puebla, M. A. Correa-Duarte, *J. Am. Chem. Soc.* **2013**, *135*, 13616–13619.
[7] L. Liang, D. Huang, H. Wang, H. Li, S. Xu, Y. Chang, H. Li, Y.-W. Yang, C. Liang, W. Xu, *Anal. Chem.* **2015**, *87*, 2504–2510.
[8] G. C. Phan-Quang, H. K. Lee, I. Y. Phang, X. Y. Ling, *Angew. Chem. Int. Ed.* **2015**, *54*, 9691–9695; *Angew. Chem.* **2015**, *127*, 9827–9831.
[9] Z. Y. Bao, D. Y. Lei, R. Jiang, X. Liu, J. Dai, J. Wang, H. L. W. Chan, Y. H. Tsang, *Nanoscale* **2014**, *6*, 9063–9070.
[10] a) Y.-F. Huang, M. Zhang, L.-B. Zhao, J.-M. Feng, D.-Y. Wu, B. Ren, Z.-Q. Tian, *Angew. Chem. Int. Ed.* **2014**, *53*, 2353–2357; *Angew. Chem.* **2014**, *126*, 2385–2389; b) X. Wang, J.-H. Zhong, M. Zhang, Z. Liu, D.-Y. Wu, B. Ren, *Anal. Chem.* **2016**, *88*, 915–921.
[11] a) L.-P. Wang, A. Titov, R. McGibbon, F. Liu, V. S. Pande, T. J. Martínez, *Nat. Chem.* **2014**, *6*, 1044–1048; b) H. Ko, S. Singamaneni, V. V. Tsukruk, *Small* **2008**, *4*, 1576–1599.
[12] W. Fan, Y. H. Lee, S. Pedireddy, Q. Zhang, T. Liu, X. Y. Ling, *Nanoscale* **2014**, *6*, 4843–4851.
[13] W. Gregory, J. M. Sanders, *Handbook of Organic Chemistry: For the Use of Students*, A. S. Barnes & Company, **1857**.
[14] D. Shechter, H. L. Dormann, C. D. Allis, S. B. Hake, *Nat. Protoc.* **2007**, *2*, 1445–1457.
[15] R. A. Ando, N. P. W. Pieczonka, P. S. Santos, R. F. Aroca, *Phys. Chem. Chem. Phys.* **2009**, *11*, 7505–7508.
[16] R. G. Pearson, *J. Chem. Educ.* **1968**, *45*, 581–587.
[17] W. Xie, B. Walkenfort, S. Schlücker, *J. Am. Chem. Soc.* **2013**, *135*, 1657–1660.
[18] P. Atkins, J. de Paula, *Atkins' Physical Chemistry*, OUP Oxford, **2010**.
[19] Y. Wang, Z. Yu, W. Ji, Y. Tanaka, H. Sui, B. Zhao, Y. Ozaki, *Angew. Chem. Int. Ed.* **2014**, *53*, 13866–13870; *Angew. Chem.* **2014**, *126*, 14086–14090.

Received: March 15, 2016
Revised: April 10, 2016
Published online: May 30, 2016

